

First-principles investigation of organic semiconductors for thermoelectric applications

Dong Wang, Ling Tang, Mengqiu Long, and Zhigang Shuai

Citation: *The Journal of Chemical Physics* **131**, 224704 (2009); doi: 10.1063/1.3270161

View online: <https://doi.org/10.1063/1.3270161>

View Table of Contents: <http://aip.scitation.org/toc/jcp/131/22>

Published by the [American Institute of Physics](#)

Articles you may be interested in

[Thermoelectric and bulk mobility measurements in pentacene thin films](#)

Applied Physics Letters **98**, 093303 (2011); 10.1063/1.3556622

[Field-effect modulated Seebeck coefficient measurements in an organic polymer using a microfabricated on-chip architecture](#)

APL Materials **2**, 032102 (2014); 10.1063/1.4867224

[Improved thermoelectric performance of organic thin-film elements utilizing a bilayer structure of pentacene and 2,3,5,6-tetrafluoro-7,7,8,8-tetracyanoquinodimethane \(F₄-TCNQ\)](#)

Applied Physics Letters **96**, 253304 (2010); 10.1063/1.3456394

[Thermoelectric properties of n-type C₆₀ thin films and their application in organic thermovoltaic devices](#)

Applied Physics Letters **99**, 093308 (2011); 10.1063/1.3631633

[Accurate on-chip measurement of the Seebeck coefficient of high mobility small molecule organic semiconductors](#)

APL Materials **3**, 096104 (2015); 10.1063/1.4931750

[Understanding electrical-thermal transport characteristics of organic semiconductors: Violation of Wiedemann-Franz law](#)

Journal of Applied Physics **120**, 195108 (2016); 10.1063/1.4967997

PHYSICS TODAY

WHITEPAPERS

ADVANCED LIGHT CURE ADHESIVES

Take a closer look at what these environmentally friendly adhesive systems can do

READ NOW

PRESENTED BY
 **MASTERBOND**
ADHESIVES | SEALANTS | COATINGS

First-principles investigation of organic semiconductors for thermoelectric applications

Dong Wang,¹ Ling Tang,¹ Mengqiu Long,¹ and Zhigang Shuai^{1,2,a)}

¹Department of Chemistry, Tsinghua University, 100084 Beijing, People's Republic of China

²Key Laboratory of Organic Solids, Beijing National Laboratory for Molecular Science, Institute of Chemistry, Chinese Academy of Sciences, 100190 Beijing, People's Republic of China

(Received 3 September 2009; accepted 9 November 2009; published online 9 December 2009)

First-principles band structure calculations coupled with the Boltzmann transport theory are used to study the thermoelectric properties in pentacene and rubrene crystals. In the constant relaxation time and rigid band approximations, the electronic contribution to the Seebeck coefficient is obtained. The absolute value of Seebeck coefficient and its temperature and carrier density dependences are in quantitative agreement with the recent field-effect-modulated measurement. The dimensionless thermoelectric figure of merit is further evaluated based on the calculated transport coefficients and experimental parameters. The peak values of figure of merit in pentacene fall in the range of 0.8–1.1, which are close to those of the best bulk thermoelectric materials. Our investigations show that organic semiconductors can be potentially good thermoelectric materials for near-room-temperature applications. © 2009 American Institute of Physics.

[doi:10.1063/1.3270161]

I. INTRODUCTION

Organic semiconductors form the material basis for the rapidly developing field of organic electronics.¹ The transport of charge and energy in organic semiconductors is fundamental to the operation of organic electronic devices, therefore has attracted continuous research interest over the last several decades. When a temperature gradient is applied to a material, charge carriers move while carrying charge as well as heat, producing a voltage gradient. This property, known as the Seebeck effect, is the basis of thermoelectric power generation. As a basic transport property of solids, the Seebeck measurement can unravel the nature and dynamics of charge transport in organic molecular crystals. Recently, the Seebeck coefficient in thin films of pentacene and single crystals of rubrene has been successfully measured using field-effect devices at the temperature between 295 and 200 K.² The measured Seebeck coefficient falls into the range of 0.3–1 mV K⁻¹, and decreases logarithmically with increasing gate voltage. Earlier measurements on thermal transport properties in pentacene thin films and rubrene single crystals show room-temperature thermal conductivities of the order of 0.5 W m⁻¹ K⁻¹.^{3,4} The relatively large Seebeck coefficient and low thermal conductivity indicate that these organic semiconductors can be potentially good thermoelectric materials.

Thermoelectrics interconvert heat and electrical energy for power generation or refrigeration. Current applications of thermoelectric generators and coolers, however, are severely hindered by the limited efficiency of thermoelectric materials, quantified by the thermoelectric figure of merit. The dimensionless thermoelectric figure of merit $zT = S^2 \sigma T / \kappa$ of a

material is determined by its Seebeck coefficient S , electrical conductivity σ , and thermal conductivity $\kappa = \kappa_e + \kappa_L$ with both the lattice and electronic contributions. To maximize the thermoelectric efficiency of a material, a large Seebeck coefficient, high electrical conductivity, and low thermal conductivity are required. As these material properties are interrelated and conflicting, a number of parameters such as carrier concentration, effective mass of charge carriers, and the electronic and lattice thermal conductivities need to be optimized to maximize zT . By far the most widely used thermoelectric materials are alloys of Bi₂Te₃ and Sb₂Te₃, with peak zT values typically in the range of 0.8–1.1.⁵ Recent advances in thermoelectrics demonstrate that complexity and disorder within the unit cell as well as nanostructured materials can lead to enhanced efficiency due to enhanced Seebeck coefficient and reduced thermal conductivity.⁶ Complex bulk materials such as skutterudites, clathrates, and Zintl phases have been explored and high efficiencies could indeed be obtained. Organic semiconductors have shown promising thermoelectric properties, but have drawn little attention in the search for novel thermoelectric materials. The aim of this investigation is to examine the potential of organic molecular thermoelectrics based on first-principles band structure calculations and the Boltzmann transport theory.

Discovery and design of optimal, cost-effective materials often require concerted efforts from both experimentalists and theorists to characterize the properties of new targeted materials.⁷ Direct efficiency measurements of thermoelectrics require nearly as much efforts as building an entire device. Measurements of contributing properties individually often introduce various uncertainties and results can vary significantly. First-principles modeling and simulations of materials behavior have played an increasingly important

^{a)}Author to whom correspondence should be addressed. Electronic mail: zgshuai@tsinghua.edu.cn.

role in materials sciences. Indeed, renewed interest in thermoelectrics beginning in the mid-1990s is motivated by theoretical predictions that thermoelectric efficiency could be greatly enhanced by quantum confinement of the electron charge carriers. In the past decade, the first-principles electronic structure calculations and the Boltzmann transport theory have been combined and applied successfully to predict the optimum doping level in established thermoelectric materials, and to discover new materials for thermoelectric applications.^{8–11} Due to the advances of modern quantum-chemical and computational techniques, it is now possible to compute the band structure of relatively complex systems. In this paper, we apply the combination of first-principles electronic structure and Boltzmann transport methods to exploring the thermoelectric performance of two prototypical organic semiconductors, pentacene and rubrene. By applying the constant relaxation time approximation to the Boltzmann equation, we have obtained the absolute value of the Seebeck coefficient and its carrier concentration and temperature dependences.

The organization of the paper is as follows. Section II briefly summarizes the theoretical methods and computational parameters used in our calculations. Detailed results of the band structures, the Seebeck coefficients, and the thermoelectric figures of merit are presented and discussed in Sec. III. Main conclusions are drawn in Sec. IV.

II. METHODOLOGY

A. Boltzmann transport theory

To evaluate the transport coefficients, we need a microscopic model of the transport process. We use the semiclassical method given by the solution of Boltzmann transport equation in the relaxation time approximation. The Boltzmann formalism describes the changes of carrier distribution function induced by the electric or magnetic fields, thermal gradient, lattice phonon scattering, or defect scattering. Due to the difficulty to take into account various charge carrier scattering mechanisms, a relaxation time approximation is usually adopted. A comprehensive description of the Boltzmann transport theory in the relaxation time approximation can be found elsewhere,¹² a brief summary of formalism used in this work is provided below. In terms of group velocity

$$v_{\alpha}(i, \mathbf{k}) = \frac{1}{\hbar} \frac{\partial \varepsilon_{i, \mathbf{k}}}{\partial k_{\alpha}}, \quad (1)$$

the energy projected transport distribution (TD) tensor is defined as

$$\sigma_{\alpha\beta}(\varepsilon) = \frac{e^2}{N} \sum_{i, \mathbf{k}} \tau_{i, \mathbf{k}} v_{\alpha}(i, \mathbf{k}) v_{\beta}(i, \mathbf{k}) \delta(\varepsilon - \varepsilon_{i, \mathbf{k}}), \quad (2)$$

where N is the number of \mathbf{k} -points sampled, $\tau_{i, \mathbf{k}}$ is the band index i and wave vector \mathbf{k} dependent relaxation time, α and β are the Cartesian indices, and e is the electron charge. The electrical conductivity, Seebeck coefficient, and thermal tensors as a function of temperature, T , and chemical potential, μ , can be written as

$$\sigma_{\alpha\beta}(T, \mu) = \frac{1}{\Omega} \int \sigma_{\alpha\beta}(\varepsilon) \left[-\frac{\partial f_0(T, \varepsilon, \mu)}{\partial \varepsilon} \right] d\varepsilon, \quad (3)$$

$$S_{\alpha\beta}(T, \mu) = \frac{1}{eT\Omega\sigma_{\alpha\beta}(T, \mu)} \int \sigma_{\alpha\beta}(\varepsilon)(\varepsilon - \mu) \times \left[-\frac{\partial f_0(T, \varepsilon, \mu)}{\partial \varepsilon} \right] d\varepsilon, \quad (4)$$

$$\kappa_{\alpha\beta}^0(T, \mu) = \frac{1}{e^2 T \Omega} \int \sigma_{\alpha\beta}(\varepsilon)(\varepsilon - \mu)^2 \left[-\frac{\partial f_0(T, \varepsilon, \mu)}{\partial \varepsilon} \right] d\varepsilon, \quad (5)$$

where Ω is the volume of unit cell and f_0 is the Fermi–Dirac distribution function. The electronic thermal conductivity is defined as

$$\kappa_e = \kappa^0 - S^2 \sigma T. \quad (6)$$

In this work, τ is simplified as an energy-independent constant. It is noted that the absolute value of S is obtained with this simplification, whereas σ and κ_e can only be calculated with respect to τ . The constant relaxation time approximation has been tested earlier and found to work quite well even for materials with highly anisotropic crystal axes.¹⁰ The essential step in the evaluation of electrical transport coefficients is to obtain the TD function, which is related to group velocities by Eq. (2). In order to obtain accurate velocities from band energies, the band interpolation method proposed by Madsen and Singh is used.^{8,13} The method has been implemented in the BoltzTrap program¹³ that can be interfaced to electronic structure packages such as WIEN2k or Vienna *ab initio* simulation package (VASP).^{9,13} To discuss the anisotropy of various transport properties, the transport tensors are output along the three crystal directions.

B. Electronic structure calculations

The first-principles band structure calculations are performed by the projector-augmented wave method¹⁴ with the Perdew–Burke–Ernzerhof generalized gradient approximation¹⁵ as implemented in VASP.¹⁶ A plane-wave cutoff energy of 400 eV and an energy convergence criterion of 10^{-4} eV for self-consistent cycle are adopted throughout calculations. The spin-orbit coupling is not considered. The atomic coordinates in the crystal structure are first relaxed with the lattice parameters fixed. For ionic relaxation and charge density calculations, a $6 \times 6 \times 4$ and $4 \times 4 \times 4$ Monkhorst–Pack \mathbf{k} -mesh¹⁷ are used for the primitive unit cell of pentacene and rubrene, respectively. The tetrahedron method with Blöchl corrections is used for smearing. For transport coefficients calculations, a much dense \mathbf{k} -mesh of $21 \times 21 \times 11$ is used for pentacene and $13 \times 13 \times 13$ for rubrene, which amounts to a total number of 2426 and 343 points in the irreducible Brillouin zone, respectively. Convergence test is also performed with denser \mathbf{k} -points. In the band structure calculations, the charge density obtained from previous self-consistent run is used and the Gaussian smearing method with a width of 0.05 eV is applied.

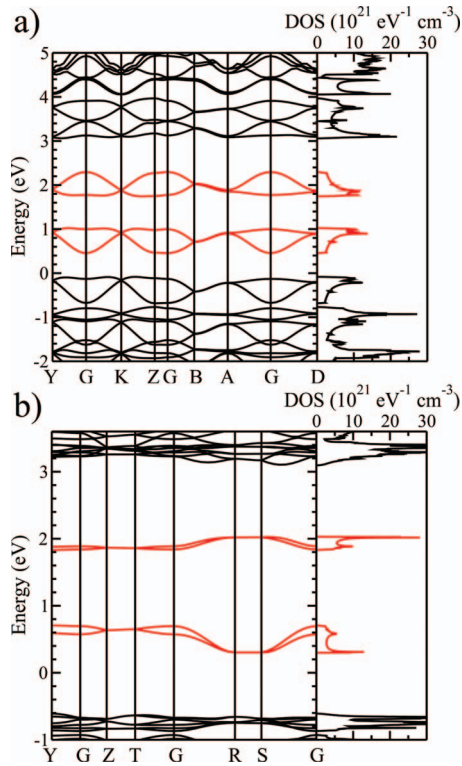


FIG. 1. The band structures and DOS of (a) pentacene and (b) rubrene. The reciprocal coordinates of high-symmetry points are $\Gamma=(0,0,0)$, $Y=(0.5,0,0)$, $B=(0,0.5,0)$, $Z=(0,0,0.5)$, $A=(0.5,0.5,0)$, $D=(0.5,0.5,-0.5)$, and $K=(0.5,0,0.5)$, respectively, in pentacene and $\Gamma=(0,0,0)$, $Y=(0.5,0.5,0)$, $Z=(0,0,0.5)$, $T=(0.5,0.5,0.5)$, $R=(0,0.5,0.5)$, and $S=(0,0.5,0)$, respectively, in rubrene. The subbands of the highest VB and lowest CB as well as their DOS are highlighted in red.

III. RESULTS AND DISCUSSION

A. Band structures

Pentacene is known to crystallize in at least four polymorphs. The band structures of pentacene single crystal phases with a d spacing of 14.5 and 14.1 Å have been studied earlier within the density functional framework.¹⁸ The substrate-induced 15.4 Å polymorph is the most relevant to organic thin-film transistor applications and is adopted in the

current investigation. The lattice parameters of pentacene thin-film phase on SiO₂ are $a=5.958$ Å, $b=7.596$ Å, $c=15.61$ Å, $\alpha=81.25^\circ$, $\beta=86.56^\circ$, and $\gamma=89.80^\circ$.¹⁹ Rubrene crystallizes in the orthorhombic structure with lattice parameters of $a=26.86$, $b=7.19$, and $c=14.43$ Å.²⁰ The crystal structure of these materials is characterized by the in-plane herringbone arrangement of two inequivalent molecules and the layered structure of molecules in the perpendicular direction. The band structures and density of states (DOS) of pentacene and rubrene are depicted in Fig. 1. The reciprocal coordinates of high-symmetry points are $\Gamma=(0,0,0)$, $Y=(0.5,0,0)$, $B=(0,0.5,0)$, $Z=(0,0,0.5)$, $A=(0.5,0.5,0)$, $D=(0.5,0.5,-0.5)$, and $K=(0.5,0,0.5)$, respectively, in pentacene and $\Gamma=(0,0,0)$, $Y=(0.5,0.5,0)$, $Z=(0,0,0.5)$, $T=(0.5,0.5,0.5)$, $R=(0,0.5,0.5)$, and $S=(0,0.5,0)$, respectively, in rubrene. Since the crystal structure of these compounds contains two molecules in a unit cell, each band in the band structures appears in pair. Band dispersions of the two subbands of the highest valence band (VB) and the lowest conduction band (CB) along high-symmetry directions are provided in Table I. The hole transport behavior is governed by the structural feature of the highest VB. A rather dispersed lower subband and a relatively flat upper subband are noted in the highest VB of pentacene. In contrast, the band splitting in the highest VB of rubrene is quite small. Consequently, the DOS in pentacene exhibits a sharp peak at the top of the VB whereas the DOS distribution at the top of VB is relatively smooth in rubrene. As will be seen below, for highly doped semiconductors, the magnitude of the Seebeck coefficient is determined by the DOS distribution around the Fermi level. Sharper distribution of DOS leads to larger Seebeck coefficient.

B. Seebeck coefficient

The Seebeck coefficient calculated as a function of carrier concentration at room temperature is plotted in Fig. 2(a) along with the experimental data.² The carrier concentration N is defined as the difference between the hole concentration,

TABLE I. Band dispersions of the two subbands in the highest VB and lowest CB of pentacene and rubrene. The reciprocal coordinates of the high-symmetry points Γ , Y , B , Z , and A in pentacene are (0,0,0), (0.5,0,0), (0,0.5,0), (0,0,0.5), and (0.5,0.5,0), respectively, those of Γ , Y , Z , T , and R in rubrene are (0,0,0), (0.5,0.5,0), (0,0,0.5), (0.5,0.5,0.5), and (0,0.5,0.5), respectively.

		Band dispersion (meV)				
		ΓY	ΓB	ΓZ	ΓA	Whole band
Pentacene	VB2	468	253	10	445	468
	VB1	99	282	15	82	306
	CB1	121	244	25	77	274
	CB2	386	263	24	407	426
		ΓY	ΓZ	ΓT	ΓR	Whole band
Rubrene	VB2	16	61	75	270	345
	VB1	10	61	47	393	403
	CB1	8	26	20	181	190
	CB2	6	22	29	133	168

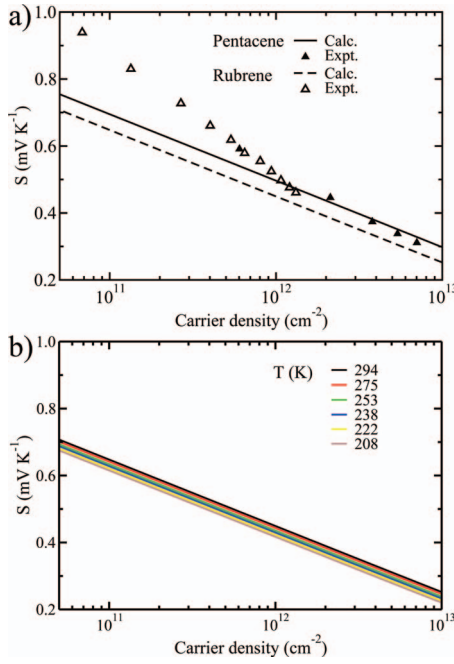


FIG. 2. The Seebeck coefficient calculated as a function of carrier concentration (a) for pentacene and rubrene at room temperature and compared to the field-effect transistor measurements. The calculated Seebeck data have been averaged over three crystal directions (b) for rubrene at temperatures in the range between 200 and 300 K.

$$N_p = 2 \int_{\text{VB}} g(\varepsilon) [1 - f_0(T, \varepsilon, \mu)] d\varepsilon, \quad (7)$$

and the electron concentration,

$$N_n = 2 \int_{\text{CB}} g(\varepsilon) f_0(T, \varepsilon, \mu) d\varepsilon, \quad (8)$$

where $g(\varepsilon)$ is the DOS. Field-effect-modulated thermopower measurements have been realized recently on crystalline organic semiconductors.^{2,21} In the field-effect transistor (FET) structure, field-induced charge carriers move along the interface between the organic semiconductor and the dielectric gate, so conduction occurs at the surface of the semiconductor.²² Semiquantitative agreement has, however, been found between carrier mobilities obtained from FET measurements and models developed for bulk transport. In the field-effect-modulated thermopower measurements, the influence of the gate insulator or the treatment of the gate insulator on S is not obvious, suggesting that the underlying mechanisms represent intrinsic properties of organic semiconductors. In order to compare to the Seebeck coefficient measured in the FET geometry, our calculated carrier concentration is converted to the carrier density at the surface of semiconductors by multiplying the thickness of the conduction channel, T_{int} . The value of T_{int} is taken as 15 Å for pentacene as done in the literature²³ and 27 Å for rubrene, which corresponds to approximately two molecular layers. The calculated S is found to decrease linearly with E_F as the Fermi-level position shifts from the middle of the band gap downward into the VB. At the same time, carrier concentration increases exponentially with E_F . As a result, the Seebeck coefficient decreases logarithmically with increasing carrier

concentration, in agreement with the experimental observations.² However, Fig. 2(a) shows that S decreases at a different rate from the measurement. Since charge carriers fill the available states at E_F at a rate determined by the DOS, different rates between calculations and measurements actually reflect different DOSs. One has to bear in mind that the DOS calculated in a perfect crystal is different from that appears in a real material at the interface of semiconductor and dielectric gate. As the Fermi-level position moves deep into the VB where the influence of in-gap trap states is insignificant, better agreement is achieved.

The Seebeck coefficient in pentacene is slightly larger than that in rubrene. It can be understood from the different shapes of the DOS of these two compounds and the Mott formula,²⁴

$$S = \frac{\pi^2 k_B^2 T}{3e} \left. \frac{d \ln \sigma(\varepsilon)}{d\varepsilon} \right|_{E_F}, \quad (9)$$

which shows that the Seebeck coefficient is sensitive to the energy derivative of the conductivity. The sharp features in the DOS of pentacene, therefore, increase the Seebeck coefficient for a given carrier concentration and conductivity. The enhanced Seebeck coefficient in pentacene is essentially a result of the upper flat subband in the highest VB, which leads to sharp DOS. One feature noticed for the Seebeck coefficient is that unlike the electrical conductivity which is highly anisotropic, the Seebeck coefficient is almost isotropic. Since the Seebeck coefficient is defined as the ratio of the 0th and 1st moments of the electrical conductivity, the anisotropy of the Seebeck coefficient is not as pronounced as that of the electrical conductivity due to the cancellation effect. The temperature influence on the Seebeck coefficient has also been studied in the range of temperature between 200–300 K. The Seebeck coefficient calculated as a function of carrier concentration at different temperatures is shown in Fig. 2(b) for rubrene. It can be seen that the overall influence of temperature is insignificant as observed in the experiment.²

C. Theoretical thermoelectric figure of merit zT

The Seebeck coefficient S , electrical conductivity σ , thermoelectric power factor $S^2\sigma$, electronic thermal conductivity κ_e , and the dimensionless figure of merit $zT = S^2\sigma T / (\kappa_e + \kappa_L)$ are plotted as a function of the carrier concentration at room temperature in Fig. 3. As mentioned earlier, only the absolute value of S is obtained in the constant relaxation time approximation; other transport properties are obtained with respect to τ . Figure 3 shows that at low carrier concentration, the Seebeck coefficient is large, but the electrical conductivity is low, and vice versa at high carrier concentration. Therefore there exists an optimum doping level at which the value of zT is maximized. To evaluate zT , the lattice thermal conductivity κ_L and the relaxation time τ have to be supplied as parameters. The thermal conductivity has been measured in pentacene thin films and rubrene single crystals, which is of the order of $0.5 \text{ W m}^{-1} \text{ K}^{-1}$ at room temperature for both compounds.^{3,4} We then take the measured thermal conductivity as the upper limit of the lattice

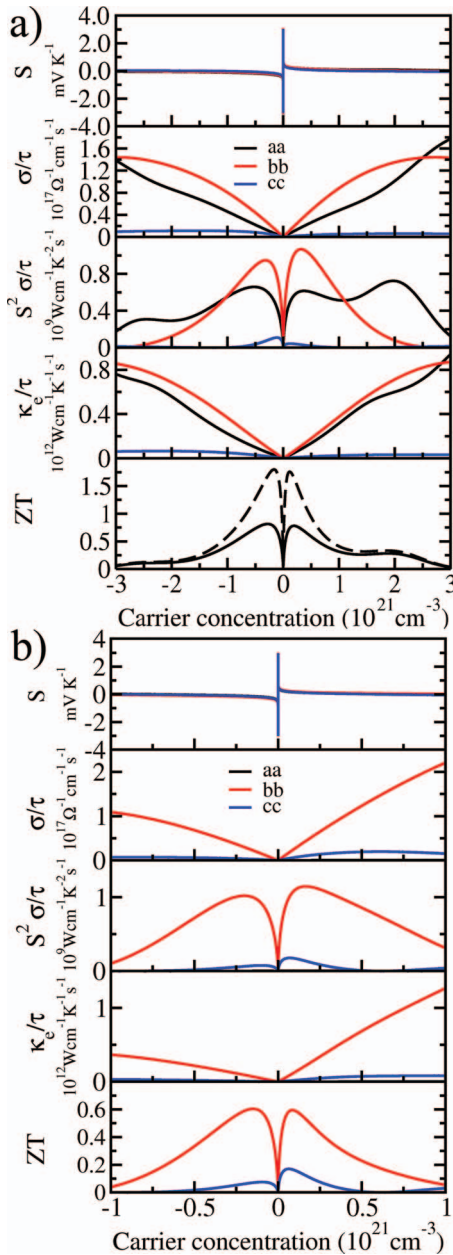


FIG. 3. The calculated transport properties and the evaluated zT values as a function of carrier concentration at room temperature: (a) pentacene. zT is estimated with the calculated transport coefficients along the a crystal direction and the supplied parameters: $\tau=31$ fs, $\kappa_L=0.51 \text{ W m}^{-1} \text{ K}^{-1}$ in solid line and alternatively $\tau=97$ fs, $\kappa_L=0.51 \text{ W m}^{-1} \text{ K}^{-1}$ in dashed line. (b) rubrene. zT along the b and c crystal axes is evaluated, respectively, based on the calculated transport coefficients and supplied parameters of $\tau_b=12$ fs, $\tau_c=17$ fs, and $\kappa_L=0.5 \text{ W m}^{-1} \text{ K}^{-1}$.

thermal conductivity, and add to it the calculated electronic contribution to obtain the overall thermal conductivity. The magnitude of charge carrier mobility μ with respect to τ is obtained through the relation $\sigma=\mu eN$. The relaxation time τ is then derived by fitting available experimental mobilities to our calculated values. The temperature dependence of hole mobility in ultrapure pentacene crystals has been extracted from the space charge-limited current measurements.²⁵ At room temperature, a mobility of $11.2 \text{ cm}^2 \text{ V}^{-1} \text{ s}^{-1}$ is obtained assuming a uniform current distribution across the crystal, whereas a mobility of $35 \text{ cm}^2 \text{ V}^{-1} \text{ s}^{-1}$ is extracted

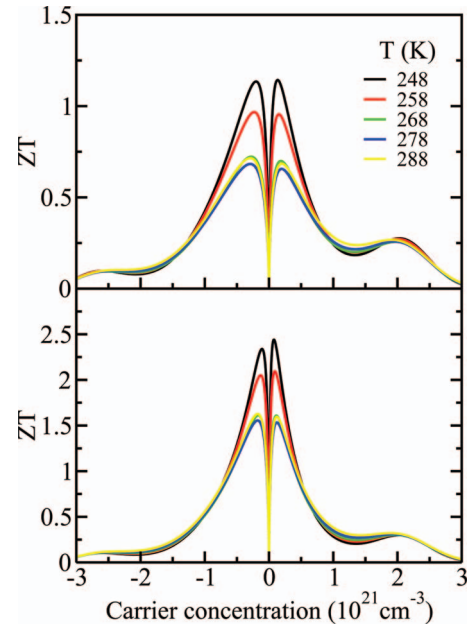


FIG. 4. zT evaluated at different temperatures for pentacene based on the calculated transport coefficients along the a crystal direction and τ and κ_L derived from experimental data. τ is derived from the temperature dependence of mobility $\mu \sim T^{-2.38}$ with $\mu=11.2$ (upper panel) and $35 \text{ cm}^2 \text{ V}^{-1} \text{ s}^{-1}$ (lower panel) at room temperature, respectively.

assuming a factor of 10^2 anisotropy of conductivity along the a and c axes.²⁵ The relaxation time is estimated to be 31 and 97 fs, respectively, by fitting the experimental data to the calculated mobility along the a crystal direction. The magnitude of zT is evaluated based on the calculated transport properties along the a crystal direction. It exhibits a peak value of 0.8 at the carrier concentration of $2 \times 10^{20} \text{ cm}^{-3}$ for $\tau=31$ fs, whereas a peak value of 1.8 at the carrier concentration of $1 \times 10^{20} \text{ cm}^{-3}$ for $\tau=97$ fs. The temperature dependence of charge carrier mobility and thermal conductivity in pentacene has been well characterized experimentally,^{3,25} which allows us to evaluate the temperature dependent thermoelectric figure of merit. The measured hole mobility exhibits a power law dependence on the temperature $\mu \sim T^{-2.38}$ with $\mu=11.2$ or $35 \text{ cm}^2 \text{ V}^{-1} \text{ s}^{-1}$ at room temperature.²⁵ The temperature dependent relaxation time can be derived in a similar way as described above. The measured thermal conductivity also displays a strong temperature dependence, which is $0.51 \text{ W m}^{-1} \text{ K}^{-1}$ at room temperature, peaks near 273 K with a value of $0.62 \text{ W m}^{-1} \text{ K}^{-1}$, and decreases to $0.3 \text{ W m}^{-1} \text{ K}^{-1}$ near 248 K.³ The zT - N curves at different temperatures are plotted in Fig. 4 for pentacene. At 248 K, zT exhibits a peak value of 1.1 and 2.4, evaluated, respectively, based on the room-temperature mobility of 11.2 and $35 \text{ cm}^2 \text{ V}^{-1} \text{ s}^{-1}$.

The mobility in rubrene FET extracted from four-probe measurements of the conductivity along the b and c axes is 20 and $8 \text{ cm}^2 \text{ V}^{-1} \text{ s}^{-1}$, respectively, at room temperature.²⁶ To obtain the best fit, a relaxation time of 12 and 17 fs can be derived, respectively, along the b and c axes, showing an anisotropy of scattering processes along different crystal directions. Note the relaxation times obtained for organic semiconductors are of the same order of magnitude as those of

Bi_2Te_3 , which are about 20 fs. zT along the b crystal direction exhibits a peak value of 0.6 at the carrier concentration of $8 \times 10^{19} \text{ cm}^{-3}$. In contrast to pentacene, rubrene only shows moderate thermoelectric figure of merit. The difference of zT in pentacene and rubrene can be attributed mainly to the different Seebeck coefficients in these materials at the optimum doping level. Good thermoelectrics should possess both large Seebeck coefficients and high carrier mobilities, which in turn require both flat and dispersed bands around the Fermi level. These distinctive band features have been observed in pentacene. In rubrene, the two subbands of the highest VB are as dispersed as those in pentacene but are almost degenerate, leading to reduced Seebeck coefficient.

IV. CONCLUSIONS

To conclude, we have applied the first-principles electronic structure calculations coupled with the Boltzmann transport theory to study thermoelectric effects in organic semiconductors. We have obtained the absolute value of the Seebeck coefficient in pentacene and rubrene in the constant relaxation time approximation. The electronic contribution to the Seebeck coefficient and its carrier-concentration and temperature dependences agree reasonably well with the experimental results. A peak zT value in the range of 0.8–1.8 at 294 K and 1.1–2.4 at 248 K is calculated for pentacene, depending on the choice of experimental mobility to derive the relaxation time. These figures of merit, even at the lower limit, are close to those of the state-of-the-art thermoelectric materials. It indicates that organic materials can have great potentials as thermoelectric materials for near-room-temperature applications such as environment-friendly refrigeration. Analysis of the band structures in pentacene and rubrene shows that the good thermoelectric properties rely on the simultaneous presence of both flat and dispersed bands around the Fermi level. The relationship established between electronic structures and thermoelectric properties in the current study shows that first-principles calculations coupled with Boltzmann transport theory can find wide applications in the discovery and design of complex thermoelectric materials.

ACKNOWLEDGMENTS

The authors are indebted to Professor Wenqing Zhang for insightful discussion and to Professor Daoben Zhu for suggestion and encouragements. This work is supported by the National Science Foundation of China (Grant Nos.

20833004, 20773145, and 20733006) and the Ministry of Science and Technology of China (Grant Nos. 2006CB806200, 2006CB932100, and 2009CB623600).

- ¹S. R. Forrest, *Nature (London)* **428**, 911 (2004).
- ²K. P. Pernstich, B. Rossner, and B. Batlogg, *Nature Mater.* **7**, 321 (2008).
- ³N. Kim, B. Domercq, S. Yoo, A. Christensen, B. Kippelen, and S. Graham, *Appl. Phys. Lett.* **87**, 241908 (2005).
- ⁴Y. Okada, M. Uno, and J. Takeya, *Mater. Res. Soc. Symp. Proc.* **B10**, 1154 (2009).
- ⁵G. S. Nolas, J. Sharp, and H. J. Goldsmid, *Thermoelectrics: Basic Principles and New Materials Developments* (Springer, New York, 2001).
- ⁶G. J. Snyder and E. S. Toberer, *Nature Mater.* **7**, 105 (2008); M. S. Dresselhaus, G. Chen, M. Y. Tang, R. G. Yang, H. Lee, D. Z. Wang, Z. F. Ren, J. P. Fleurial, and P. Gogna, *Adv. Mater. (Weinheim, Ger.)* **19**, 1043 (2007); A. I. Hochbaum, R. K. Chen, R. D. Delgado, W. J. Liang, E. C. Garnett, M. Najarian, A. Majumdar, and P. D. Yang, *Nature (London)* **451**, 163 (2008); A. I. Boukai, Y. Bunimovich, J. Tahir-Kheli, J. K. Yu, W. A. Goddard, and J. R. Heath, *ibid.* **451**, 168 (2008); R. Venkatasubramanian, E. Siivola, T. Colpitts, and B. O'Quinn, *ibid.* **413**, 597 (2001).
- ⁷E. A. Carter, *Science* **321**, 800 (2008).
- ⁸G. K. Madsen, *J. Am. Chem. Soc.* **128**, 12140 (2006).
- ⁹J. Yang, H. M. Li, T. Wu, W. Q. Zhang, L. D. Chen, and J. H. Yang, *Adv. Funct. Mater.* **18**, 2880 (2008).
- ¹⁰T. J. Scheidemantel, C. Ambrosch-Draxl, T. Thonhauser, J. V. Badding, and J. O. Sofo, *Phys. Rev. B* **68**, 125210 (2003).
- ¹¹X. Gao, K. Uehara, D. D. Klug, S. Patchkovskii, J. S. Tse, and T. M. Tritt, *Phys. Rev. B* **72**, 125202 (2005); J. S. Rhyee, K. H. Lee, S. M. Lee, E. Cho, S. I. Kim, E. Lee, Y. S. Kwon, J. H. Shim, and G. Kotliar, *Nature (London)* **459**, 965 (2009).
- ¹²B. R. Nag, *Electron Transport in Compound Semiconductors* (Springer-Verlag, Berlin, 1980).
- ¹³G. K. H. Madsen and D. J. Singh, *Comput. Phys. Commun.* **175**, 67 (2006).
- ¹⁴P. E. Blöchl, *Phys. Rev. B* **50**, 17953 (1994); G. Kresse and D. Joubert, *ibid.* **59**, 1758 (1999).
- ¹⁵J. P. Perdew, K. Burke, and M. Ernzerhof, *Phys. Rev. Lett.* **77**, 3865 (1996).
- ¹⁶G. Kresse and J. Furthmüller, *Phys. Rev. B* **54**, 11169 (1996).
- ¹⁷H. J. Monkhorst and J. D. Pack, *Phys. Rev. B* **13**, 5188 (1976).
- ¹⁸K. Hummer and C. Ambrosch-Draxl, *Phys. Rev. B* **72**, 205205 (2005).
- ¹⁹S. Schiefer, M. Huth, A. Dobrineski, and B. Nickel, *J. Am. Chem. Soc.* **129**, 10316 (2007).
- ²⁰O. D. Jurchescu, A. Meetsma, and T. T. Palstra, *Acta Crystallogr. Sect. B: Struct. Sci.* **62**, 330 (2006).
- ²¹A. von Mühlénen, N. Errien, M. Schaer, M. N. Bussac, and L. Zuppiroli, *Phys. Rev. B* **75**, 115338 (2007).
- ²²M. E. Gershenson, V. Podzorov, and A. F. Morpurgo, *Rev. Mod. Phys.* **78**, 973 (2006).
- ²³D. Oberhoff, K. P. Pernstich, D. J. Gundlach, and B. Batlogg, *IEEE Trans. Electron Devices* **54**, 17 (2007).
- ²⁴M. Cutler and N. F. Mott, *Phys. Rev.* **181**, 1336 (1969).
- ²⁵O. D. Jurchescu, J. Baas, and T. T. M. Palstra, *Appl. Phys. Lett.* **84**, 3061 (2004).
- ²⁶V. Podzorov, E. Menard, A. Borissov, V. Kiryukhin, J. A. Rogers, and M. E. Gershenson, *Phys. Rev. Lett.* **93**, 086602 (2004).